Journal of Zhejiang University-SCIENCE A (Applied Physics & Engineering)
ISSN 1673-565X (Print); ISSN 1862-1775 (Online)
www.zju.edu.cn/jzus; www.springerlink.com
E-mail: jzus@zju.edu.cn

Physically-based approach to analyze rainfall-triggered landslide using hydraulic gradient as slide direction*

Qi-hua RAN[1], Dan-yang SU[1], Qun QIAN[1], Xu-dong FU[2], Guang-qian WANG[1,2], Zhi-guo HE[†‡3]

([1]*Department of Hydraulic Engineering, Zhejiang University, Hangzhou 310058, China*)

([2]*State Key Laboratory of Hydroscience and Engineering, Tsinghua University, Beijing 100084, China*)

([3]*Department of Ocean Science and Engineering, Zhejiang University, Hangzhou 310058, China*)

[†]E-mail: hezhiguo@zju.edu.cn

Received Feb. 28, 2012; Revision accepted Aug. 16, 2012; Crosschecked Sept. 31, 2012

Abstract: An infinite slope stability numerical model driven by the comprehensive physically-based integrated hydrology model (InHM) is presented. In this approach, the failure plane is assumed to be parallel to the hydraulic gradient instead of the slope surface. The method helps with irregularities in complex terrain since depressions and flat areas are allowed in the model. The present model has been tested for two synthetic single slopes and a small catchment in the Mettman Ridge study area in Oregon, United States, to estimate the shallow landslide susceptibility. The results show that the present approach can reduce the simulation error of hydrological factors caused by the rolling topography and depressions, and is capable of estimating spatial-temporal variations for landslide susceptibilities at simple slopes as well as at catchment scale, providing a valuable tool for the prediction of shallow landslides.

Key words: Shallow landslide, Infinite slope stability model, Hydraulic gradient, Physically-based hydrology model, Integrated hydrology model (InHM)

doi:10.1631/jzus.A1200054 **Document code:** A **CLC number:** TV1

1 Introduction

Shallow landslide is defined by a sliding surface within the soil mantle or weathered bedrock, typically a few decimeters to several meters deep. Shallow landslide is usually triggered when pore water pressures are high enough to reduce effective normal stress to a critical level (Renwick, 1982). The controlling factors for the shallow landslide hazard are usually categorized as geological (e.g., materials), morphological (e.g., slope angle), physical (e.g., rainfall, earthquake), and human-associated factors (e.g., land use change, water management). Some factors make the slope vulnerable to failure and predispose the slope to potential instability, while others more directly initiate landslide.

Shallow landslide models usually include two main components: a hydrology model and a slope stability model. A considerable number of physically-based models have been developed to assess shallow landslide hazard, which can be classified into four groups: models based on Montgomery and Dietrich (1994)'s approach (Montgomery and Dietrich, 1994; Montgomery *et al*., 2000; Guimaraes *et al*., 2003; Fernandes *et al*., 2004; Chang, 2007; Lee *et al*., 2009; Minder *et al*., 2009), models based on Iverson (2000)'s approach (Iverson, 2000; Baum *et al*., 2002; Chen *et al*., 2005; Rosso *et al*., 2006; Tsai and Yang, 2006; Tsai *et al*., 2008), models based on Système

‡ Corresponding author

* Project supported by the National Basic Research Program (973) of China (No. 2011CB409901-01), and the Foundation of Science and Technology Department of Zhejiang Province (No. 2009C33117), China

Hydrologique Européen (SHE) hydrological modelling system (Burton and Bathurst, 1998; Bathurst *et al*., 2005; Bovolo and Bathurst, 2011), and models based on other alternative approaches (Beville *et al*., 2010; Ebel *et al*., 2010). The major difference of these approaches relies on the different equation forms and solution algorithm in the hydrology models.

The above mentioned models use an infinite slope stability model in calculating the factor of safety, where the failure plane is assumed to be parallel to the surface slope. The problem is that the failure surface does not necessarily follow the topography, especially if the topography is described by very-high resolution digital elevation model (DEM) with depressions. The predicted slope stability results are strongly influenced by the resolution, accuracy and reliability of the elevation data from the DEM (Dietrich *et al*., 1998; Claessens *et al*., 2005). Keeping the original topographic characteristics such as depressions and flat regions could be important in landslide assessment. However, to the authors' knowledge, no slope stability model is available at present that considers depressions and flat areas in high resolution DEM that provides the correct slide direction. It is the authors' opinion that an alternative approach, which can keep the original terrain when evaluating slope stability, is needed. The hydraulic gradient, usually equal to the gradient of the ground water table, is a representation of the terrain feature. It provides surface slope characteristics and alleviates the effect of local depressions and flat regions. Therefore, in the present approach, the failure plane is assumed to be parallel to the hydraulic gradient instead of the surface slope in the revised infinite slope stability model.

Since soil water saturation plays a critical role in the occurrence of landslide, any approach that aims at predicting landslide effectively must be able to estimate soil water movement correctly. The comprehensive physically based integrated hydrology model (InHM) (VanderKwaak, 1999) was employed to simulate detailed soil water saturation and pressure head field, which were then used to drive the revised infinite slope stability model. The present approach was tested for two simple slopes and a small catchment in the Mettman Ridge study area in Oregon, United States, to estimate the shallow landslide susceptibility.

2 Hydrology model

The InHM was originally designed by VanderKwaak (1999) to quantitatively estimate, in a fully coupled approach, water flow and solute transport within a spatially variable porous medium (with or without fractures and/or macrospores) and across the land surface above and adjacent to the subsurface. Testing and applications of InHM have been widely reported since 1999 (VanderKwaak and Loague, 2001; Loague and VanderKwaak, 2002; Loague *et al*., 2004; Ran, 2006; Ran *et al*., 2007; Ebel and Loague, 2008; Ebel *et al*., 2008; 2009; Heppner and Loague, 2008; Mirus *et al*., 2009; Ran *et al*., 2012). The flexibility of InHM has facilitated successful simulation of hydrologic response for a variety of catchment sizes and hydrologic environments.

A brief outline of the subsurface and surface flow components of InHM is presented in the following paragraphs. A complete description of the coupled surface/subsurface flow equations and detailed discussion of the solution methods are referred to VanderKwaak (1999).

3D subsurface flow in variably saturated porous medium is simulated in InHM by

$$\nabla \cdot \boldsymbol{q} \pm q^{\mathrm{b}} \pm q_{\mathrm{ps}}^{\mathrm{e}} = \frac{\partial \phi S_{\mathrm{w}}}{\partial t}, \tag{1}$$

where $\boldsymbol{q}$ is the Darcy flux, m/s, q^{b} is a specified rate source/sink, s^{-1}, $q_{\mathrm{ps}}^{\mathrm{e}}$ (equals $-q_{\mathrm{sp}}^{\mathrm{e}}$) is the rate of water exchange between the porous medium and surface continua, s^{-1}, ϕ is the porosity, S_{w} is the water saturation, and t is the time, s. The Darcy flux in Eq. (1) is given by

$$\boldsymbol{q} = -k_{\mathrm{rw}} \frac{\rho_{\mathrm{w}} g}{\mu_{\mathrm{w}}} \boldsymbol{k} \nabla(\psi_{\mathrm{p}} + z), \tag{2}$$

where k_{rw} is the relative permeability, ρ_{w} is the water density, $\mathrm{m/L^3}$, $\boldsymbol{k}$ is the intrinsic permeability vector, m^2, ψ_{p} is the pressure head, m, z is the elevation head, m, and μ_{w} is the viscosity of water, kg/(m·s).

The transient flow of water on the land surface (both overland and open channel) is estimated by the diffusion wave approximation of the depth-averaged shallow water equations. Such 2D surface flow is

conceptualized as a second continuum that interacts with the underlying variably saturated porous medium through a thin soil layer of thickness a_s, m. Assuming a negligible influence of inertial forces and a shallow depth of water, Ψ_s, m, the conservation of water on the land surface, is described by

$$\nabla\cdot\psi_s^{\text{mobile}}\boldsymbol{q}_s \pm a_s q^b \pm a_s q_{sp}^e = \frac{\partial(S_{w_s}h_s+\psi_s^{\text{store}})}{\partial t}, \quad (3)$$

where $\boldsymbol{q}_s$ is the surface water velocity, m/s, and S_{w_s} is the surface saturation, defined as

$$\begin{aligned} &S_{w_s} = \psi_r^{2(1-\psi_r)},\\ &\psi_r = \min\{1,\max\{0,\psi_s/h_s\}\}, \end{aligned} \quad (4)$$

where Ψ_r is the surface water depth, m, relative to the average height of surface micro-topography h_s, m. ψ_s^{store} and ψ_s^{mobile} are stored and mobile are water depths, m, defined as

$$\begin{cases} \psi_s^{\text{store}} = \max\{0,\psi_s - h_s\},\\ \psi_s^{\text{mobile}} = \max\{0,\psi_s - \psi_s^{\text{pond}}\}, \end{cases} \quad (5)$$

where ψ_s^{pond} is the depth of pond water that does not participate in overland flow (e.g., depression storage), m. Surface water velocities are calculated using a 2D form of the empirical, though well-established, and the Manning water depth/friction-discharge equation can be given by

$$\boldsymbol{q}_s = -\frac{(\psi_s^{\text{mobile}})^{2/3}}{n\Phi^{1/2}}\nabla(\psi_s+z), \quad (6)$$

where n is the Manning's surface roughness tensor, $s\cdot m^{-1/3}$, and Φ is the energy slope approximated as

$$\Phi = \left[\left(\frac{\partial(\psi_s+z)}{\partial x}\right)^2 + \left(\frac{\partial(\psi_s+z)}{\partial y}\right)^2\right]^{0.5}. \quad (7)$$

The linkages between different components of InHM are through first-order, physically-based flux relationships driven by pressure head gradients.

Surface/subsurface water exchange rates q_{sp}^e, s^{-1} are approximated as

$$q_{sp}^e = \alpha^e(\psi_p - \psi_s) = -q_{ps}^e, \quad (8)$$

where α^e is the nonlinear water exchange coefficient, $(m\cdot s)^{-1}$, given by

$$\alpha^e = k_{rw}^e\frac{\rho_w g}{\mu_w}\frac{k_p^{zz}}{a_s^2}, \quad (9)$$

where k_p^{zz} is the permeability of the porous media, m/s. The interface relative permeability, k_{rw}^e, which ensures that the discretized solution is monotone, is defined in the upstream continuum as

$$k_{rw}^e = \begin{cases} k_{rw_p}, \psi_p \ge \psi_s,\\ k_{rw_s}, \psi_p < \psi_s, \end{cases} \quad (10)$$

where k_{rw_p} is the relative permeability of the porous medium and k_{rw_s} is the pseudo-relative permeability of the surface continuum. The surface pseudo-relative permeability is defined as being equivalent to the surface saturation in Eq. (3). Eq. (7) describes both rates of surface water infiltration and groundwater seepage (or exfiltration). Infiltration and exfiltration rates are determined by spatially and temporally variable subsurface pressure head gradients and surface water depths, and by spatially variable porous medium properties. The flows in both the surface and subsurface continua are therefore intimately coupled, and the rates of water exchange between continua are not specified but evolve in time and space as a function of local hydrodynamics (VanderKwaak, 1999).

The governing flow and transport equations are discretized in space using the control volume finite element method. Each coupled system of nonlinear equations in InHM simulation is solved implicitly using the Newton iteration (VanderKwaak, 1999). The calculated water saturation and pressure head gradients of the porous medium are used to calculate factor of safety in the slope stability model.

3 Slope stability model

The infinite slope stability model is widely used because of its simplicity and practicability. The widely accepted assumption that the failure plane is parallel to the surface slope, however, is not always adequate for rolling topography (Fig. 1). For rolling topography, water table gradient, which can be represented by hydraulic gradient, is more representative than surface slope in serving as the slide angle. It provides surface slope characteristics and alleviates the effect of local depressions and flat regions. However, no infinite slope stability model using the hydraulic gradient as slide angle, to the authors' knowledge, has been reported. From Inverson (1990)'s study of groundwater flow fields in infinite slopes, the possible flow lines seem more suitable to act as the failure plane. Kawagoe *et al*. (2010) evaluated the frequency and distribution of landslide hazards over Japan using a probabilistic model based on multiple logistic regression analysis, which suggests that the sensitivity analysis confirmed that the hydrological parameter (hydraulic gradient) is the most influential factor in the occurrence of landslides. Hydraulic gradient affects subsurface flow that has great influence on landslides. Besides, the hydraulic gradient may also affect the slide direction due to the subsurface. In this study, it is a trial that the failure plane is assumed to be parallel to the hydraulic gradient, instead of slope surface. The edge effects are neglected since the failure depth is usually much smaller than the slope length in mountainous areas (Milledge *et al*., 2012).

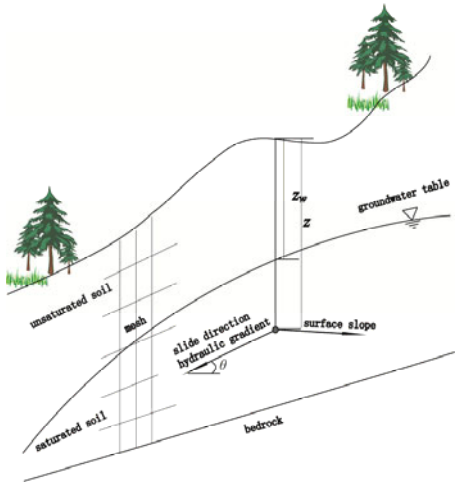

Fig. 1 1D schematic illustration of slope and landslide

The normal stress σ, kg/(m·s^2), due to the weight of a sliding mass and the soil pore-water pressure u, kg/(m·s^2), can be expressed by

$$\begin{cases}\sigma = \cos^2\theta\int_0^z \rho g\mathrm{d}z, \\ u = (z - z_w)\rho_w g\cos^2\theta, \end{cases} \tag{11}$$

where ρ is the soil density, kg/m^3, g is the gravitational acceleration, m/s^2, θ is the angle of the failure plane to the horizontal, z_w is the depth of groundwater level, m, and z is the depth of the potential failure plane, m, as shown in Fig. 1. In fact, (z–z_w) equals the pore-water pressure that can be calculated from the hydrology model InHM.

The shear strength τ_f, kg/(m·s^2), of the soil along the potential failure plane is expressed by

$$\tau_f = c' + (\sigma - u)\tan\phi', \tag{12}$$

where c' is the effective cohesion of the soil, kg/(m·s^2), and ϕ' is the effective internal friction angle for the soil or between the soil and bedrock. For vegetated sites, root systems contribute to soil strength by providing an artificial cohesion c_r, kg/(m·s^2), that can be added to effective soil cohesion in the Mohr-Coulomb equation. Then, the effects of rooting strength can be incorporated into Eq. (11) as follows:

$$\tau_f = c_r + c' + (\sigma - u)\tan\phi'. \tag{13}$$

The shear stress τ, kg/(m·s^2), of the soil along the potential failure plane is expressed by

$$\tau = \sin\theta\cos\theta\int_0^z \rho g\mathrm{d}z. \tag{14}$$

The factor of safety (FS) is expressed by

$$\mathrm{FS} = \frac{\tau_f}{\tau}. \tag{15}$$

When FS>1.0, the slope is stable; otherwise the slope is unstable.

Substituting Eqs. (11)–(14) into Eq. (15) yields the general expression for the factor of safety in the form:

$$\mathrm{FS}=\frac{c_\mathrm{r}+c'+\cos^2\theta\tan\phi'\int_0^z\rho'g\mathrm{d}z}{\sin\theta\cos\theta\int_0^z\rho g\mathrm{d}z}, \tag{16}$$

where ρ' is the submerged soil density, kg/m^3, that can be expressed by

$$\rho'=\begin{cases}\rho, & 0<h\le z_\mathrm{w},\\ \rho-\rho_\mathrm{w}, & z_\mathrm{w}<h\le z.\end{cases} \tag{17}$$

Soil density ρ, kg/m^3, can be calculated from the soil-phase conversion formula as

$$\rho=n_\mathrm{s}S_\mathrm{w}\rho_\mathrm{w}+(1-n_\mathrm{s})d_\mathrm{s}\rho_\mathrm{w}, \tag{18}$$

where d_s is the soil particle specific density, S_w is the water saturation, and n_s is the soil porosity. For all the parameters from Eqs. (16)–(18), c_r, c', ϕ', d_s and n_s are the given soil properties, S_w and θ are calculated by the hydrology model. FS is calculated from the surface to the bottom of the soil, and the depth with the lowest FS value is taken to be the potential failure depth. All the parameters and variables required for simulating slope stability is given in Table 1.

4 Numerical simulation and discussion

Two simple slopes and a catchment in the Mettman Ridge study area in Oregon, United States, were selected to test the capability of shallow landslide susceptibility assessment provided by the presented approach. A gentle slope and a depression are added to the simple slopes, to see how rolling topography affect the slope stability over rainfall and the applicability of the presented approach with the DEM without pre-processing. The simple slopes are representative of simple 2D terrain of slope scale, while the catchment in the Mettman Ridge study area is representative of 3D terrain of catchment scale.

Table 1 Parameters and variables required for simulating slope stability

Parameter	Definition (unit)	Source, simple slopes*	Source, catchment
d_s	Soil particle specific density	2.65[a]	
n_s	Soil porosity	63.6%[b]	
c_r	Root cohesion (kg/(m·s^2))	0[c]	
c'	Effective soil cohesion (kg/(m·s^2))	0[c]	
ϕ'_soil	Effective internal friction angle of soil (°)	35[d]	45[d]
ϕ'_bedrock	Effective internal friction angle between soil and bedrock (°)	30[e]	45[f]
S_w	Water saturation	Simulation, InHM	
θ	Slide angle (°)	Simulation, InHM or use surface slope	
z	Initial water table (m)	−2[g]	
k	Unsaturated hydraulic conductivity function	van Genuchten function[h]	
k_s	Saturated hydraulic conductivity (m/s)	5×10^{-5}[i]	
r	Rainfall intensity (m/s)	1.16×10^{-5} (1000 mm/d)[j]	5.79×10^{-7} (50 mm/d)[k]
t	Rainfall duration (s)	172 800 (2 d)[j]	86 400 (1 d)[k]

* The parameters for simulating simple slopes are hypothesized based on the study of shallow landslides in Coos Bay, Oregon. [a]Average of soil particle specific density for silty sand soil; [b]Calculated from bulk density based on the study (Torres *et al*., 1998); [c]Based on the studies (Schmidt *et al*., 2001; Yee and Harr, 1977); [d]Based on the studies (Iverson *et al*., 1997; Montgomery *et al*., 2009; Schmidt *et al*., 2001); [e]Based on the study (Iverson *et al*., 1997); [f]Lack of internal friction angle between soil and bedrock. The study catchment has a large area of steep slopes. If ϕ'_bedrock is set to be 30°, most of the catchment is unconditional unstable; [g]Assumption; [h]Determined by the method of van Genuchten (1980) using the parameters of α=0.075 and N=1.89 based on Torres *et al*. (1998); [i]Based on Montgomery (1991); [j]Assumption. Heavy rainfall intensity and long duration are selected to simulate unsaturated and saturated flows; [k]Based on the studies (Montgomery, 1991; Montgomery and Dietrich, 1994; Torres *et al*., 1998)

The FS simulated is estimated by theoretical analysis and compared with FS simulated by taking surface slope as slide angle. In the following paragraphs, the FS simulated by taking hydraulic gradient as slide angle is labeled as method I and FS simulated by taking surface slope as slide angle is labeled as method II.

4.1 Numerical simulation I: simple slopes

The simulations were conducted based on two simple slopes to investigate how the slope stability varies over time for different topographies.

4.1.1 Mesh structure

The finite-element meshes for the two simple slopes, i.e., single smooth slope and single rolling slope with depressions, are shown in Fig. 2. The dimensions of the meshes are 10.0 m long (y axis), 1.0 m wide (x axis) and 2.0 m deep (z axis). Both of the horizontal nodal spacings (Δx, Δy) and the vertical nodal spacing (Δz) in the mesh are 0.1 m. The total number of nodes and elements in the mesh are 16863 and 28800, respectively. The slope gradient is fixed to be 35° for both slopes and the soil volumes are the same.

4.1.2 Boundary conditions

The boundary conditions for each face of boundary value problems (Fig. 2) are as follows: impermeable (A-E-G-C, B-F-H-D, C-D-H-G, A-B-C-D and E-F-H-G) and flux (A-E-F-B). To simplify the problem, the entire subsurface domain is considered to be homogeneous and isotropic. The artificial rainfall conditions, soil properties and other information required to drive the model are summarized in Table 1.

4.1.3 Simulation results

Rolling topography and depressions play an important role in hydrologic response. As shown in Fig. 3, the hydrograph of the smooth slope has an earlier rising time of outlet flow than the rolling slope. Both the slopes represent the saturation excess runoff. Three stages can be observed from the hydrograph, which represent no outlet flow stage, rising outlet flow stage and steady outlet flow stage, respectively. Three different time snapshots taken at 10 h, 20 h, and 48 h of rainfall duration, respectively, were selected to characterize the variations of hydrologic condition and slope stability. Note that it is unusual to have "overland flow" at a site where a landslide would occur as landslide sites are typically steep and have highly permeable soil resulting in runoff generation by subsurface stormflow. In this specific case, the overland flow occurs only at the downstream outlet. It is an indication of the subsurface hydraulic condition.

As shown in Fig. 4, rolling topography and depressions result into different water infiltration that affects the distribution of water saturation. Fig. 5

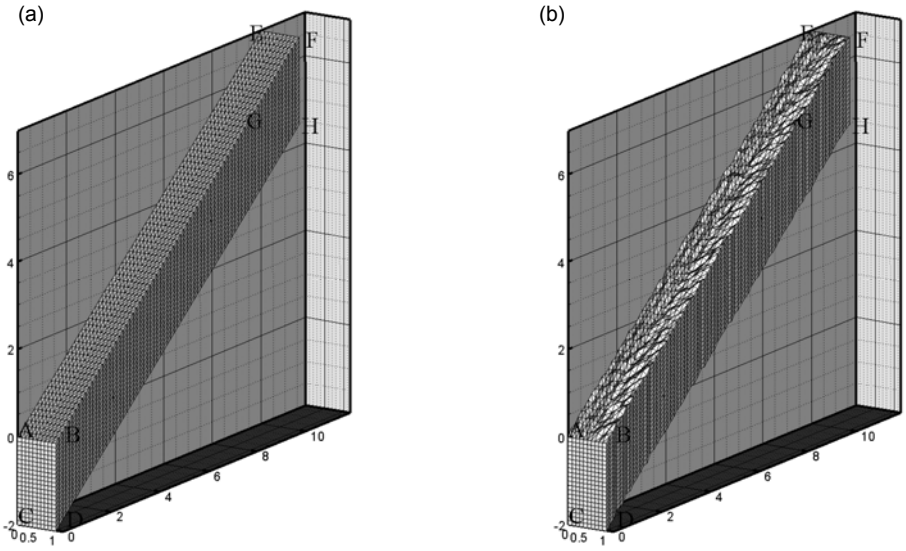

Fig. 2 Finite-element meshes used for numerical simulation I
(a) Smooth slope; (b) Rolling slope

shows simulated saturation difference distributions between the smooth slope and rolling slope at different times. Since the meshes of the smooth slope and rolling slopes were different, the saturation difference was calculated by spatial interpolation. First, the mesh of the smooth slope (S_{smooth}) was duplicated. Then the saturation value for the duplicated mesh ($S_{interpolated}$) was interpolated from the rolling slope ($S_{rolling}$) mesh by inverse-distance interpolation using eight numbers of points by octant selection. Finally, the saturation difference was calculated by $S_{interpolated}-S_{smooth}$. The saturation difference mainly appears from top soil to bottom soil as water infiltration from top to bottom. The rolling slope has larger saturation value than the smooth slope at the bottom when outlet flow is steady. Removing rolling topography and depressions will cause unrealistic distribution of water saturation which also affect the calculation of FS.

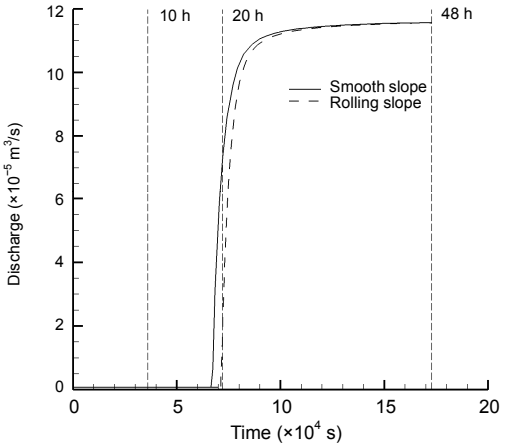

Fig. 3 Simulated hydrograph for smooth slope and rolling slope

The distribution of the simulated slide angle, defined as the hydraulic gradient calculated from total

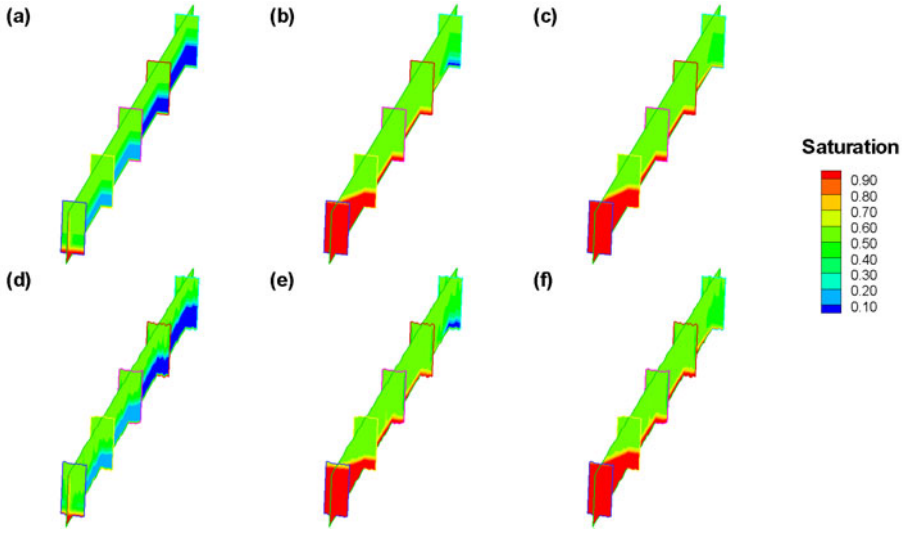

Fig. 4 Simulated saturation distributions for smooth slopes and rolling slopes

(a) Smooth slopes, t=10 h; (b) Smooth slopes, t=20 h; (c) Smooth slopes, t=48 h; (d) Rolling slopes, t=10 h; (e) Rolling slopes, t=20 h; (f) Rolling slopes, t=48 h

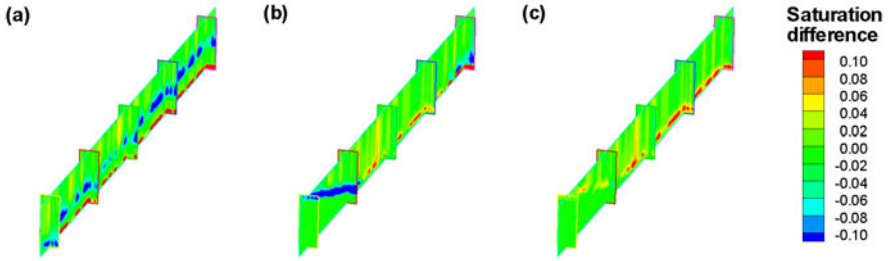

Fig. 5 Simulated saturation difference distributions between smooth slope and rolling slope at t=10 h (a), t=20 h (b), and t=48 h (c)

pressure head (method I) and surface slope (method II), is shown in Fig. 6. The slide angle distribution by method I is mainly due to the surface slope and saturation distribution. For the smooth slope, the slide angle is parallel to the surface slope except the section near the downstream end where the hydrology gradient is affected by the boundary condition. For the rolling slope, different infiltration due to rolling topography and depressions leads to some steeper hydraulic gradient at first, and the distribution of the hydraulic gradient becomes more stable as the subsoil gets saturated and water table rises. For the rolling slope, if the surface slope is taken as the slide angle, it does not vary versus water saturation, and slide angle is unrealistic in the section near the downstream end and depressions. In the specific case, the hydraulic gradient for the lower soil is predominantly horizontal due to the initial condition and then increases when the soil gets saturated. Fig. 6 suggests that, if the hydraulic gradient is taken as the slide angle, the impact of rolling topography and depressions can be reduced and the slide angle near the boundary can also be more realistic. For ideal conditions, the slide angles calculated by the hydraulic gradient and surface slope are the same.

The simulated FS distribution by method I for both smooth slope and rolling slope and that by method II for rolling slope is shown in Fig. 7. For FS simulated by method I, it can be seen that the most unstable region is the topsoil on the slope with higher water saturation before the subsoil gets saturated (Figs. 7a and 7d). When the bottom soil gets saturated, the most unstable position is located between the soil and bedrock (Figs. 7b and 7e). After the subsoil gets saturated, the FS value increases near the downstream boundary because of low hydraulic gradient and subsequently low slide angle. FS distribution simulated by method II, with the same boundary conditions for rolling slope, is shown in Figs. 7g–7i. Compared with FS by method I, the main differences of the FS distribution are as follows: (1) the subsoil is always more susceptible than (or equal to) the topsoil because the slide angle from the topsoil to subsoil is the same, and the FS of topsoil and subsoil is the

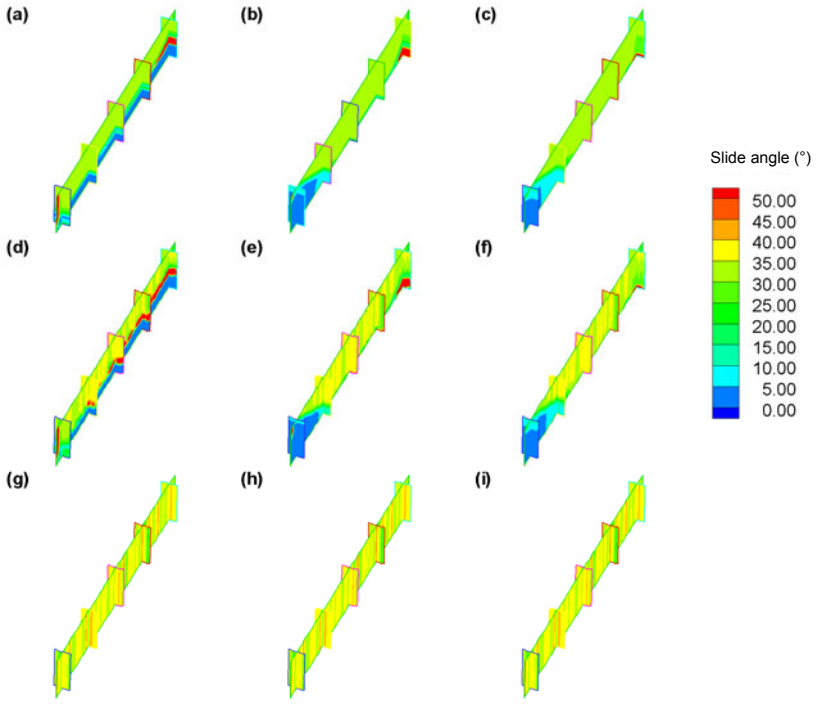

Fig. 6 Simulated slide angle distributions for smooth slopes and rolling slopes

(a) Smooth slopes by method I, t=10 h; (b) Smooth slopes by method I, t=20 h; (c) Smooth slopes by method I, t=48 h; (d) Rolling slopes by method I, t=10 h; (e) Rolling slopes by method I, t=20 h; (f) Rolling slopes by method I, t=48 h; (g) Rolling slopes by method II, t=10 h; (h) Rolling slopes by method II, t=20 h; (i) Rolling slopes by method II, t=48 h

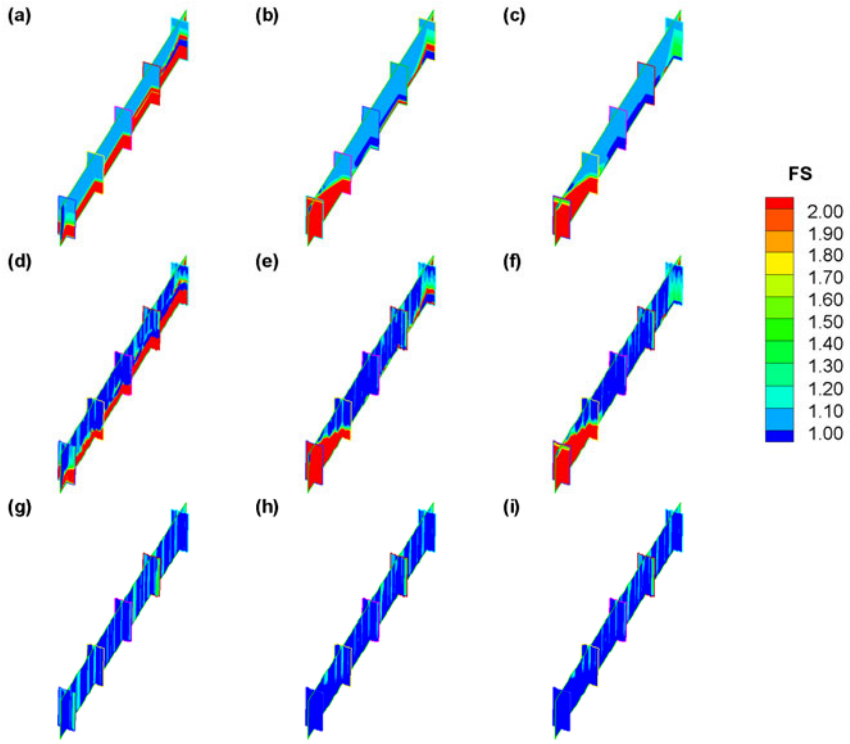

Fig. 7 Simulated FS distributions for smooth slopes and rolling slopes

(a) Smooth slopes by method I, t=10 h; (b) Smooth slopes by method I, t=20 h; (c) Smooth slopes by method I, t=48 h; (d) Rolling slopes by method I, t=10 h; (e) Rolling slopes by method I, t=20 h; (f) Rolling slopes by method I, t=48 h; (g) Rolling slopes by method II, t=10 h; (h) Rolling slopes by method II, t=20 h; (i) Rolling slopes by method II, t=48 h

same until the subsoil gets saturated; (2) the significant difference is near the downstream end where FS by method I is higher than that by method II and the boundary effect cannot be simulated by method II; and (3) the slip surface simulated is circular by method I but along the bedrock by method II.

4.2 Numerical simulation II: a catchment in Mettman Ridge

A small catchment was selected as the application site for shallow landslide assessment of catchment scale because of availability of data required to drive the reported model. The catchment, which is located along the Mettman Ridge in the Coast Range just north of Coos Bay, Oregon, USA, has an area of 0.3 km^2 with many narrow ridge tops and steep slopes. Nineteen shallow landslides occurred in the catchment between forest clearance in 1987 and the summer of 1992 (Montgomery and Dietrich, 1994). The location and the contours of the Mettman Ridge catchment are shown in Fig. 8.

4.2.1 Soil characteristics

The colluvial soil in the study area was silty sand with thickness ranging from roughly 0.1 to 0.5 m on topographic noses to greater than 2 m in topographic hollows (Montgomery, 1991). Saturated hydraulic conductivity of the colluvial soil declined from about 10^{-3} m/s at the ground surface to about 10^{-4} m/s at a depth of 2 m (Montgomery, 1991). Saturated soil bulk density was about 1600 kg/m^3 (Torres *et al.*, 1998). Several values of internal friction angle for soil developed on sandstones in the Oregon Coast Range had been reported, varying from about 35° to 44° (Yee and Harr, 1977; Schroeder and Alto, 1983; Burroughs *et al.*, 1985). Stress path analyses of low confining stress triaxial strength tests indicated the colluvial soil had a friction angle of about 40° (Iverson *et al.*, 1997; Schmidt *et al.*, 2001; Montgomery *et al.*, 2009) and was virtually cohesionless (Yee and Harr, 1977; Schmidt *et al.*, 2001; Montgomery *et al.*, 2009).

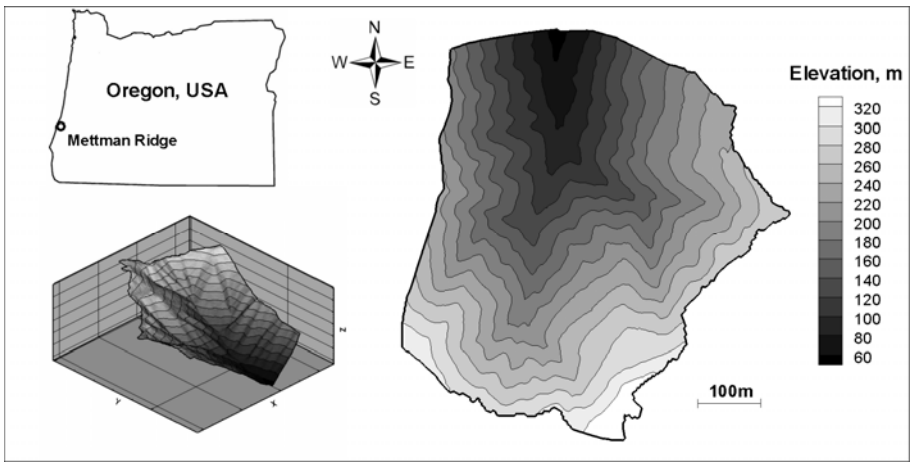

Fig. 8 Location and contour DEM of the catchment in Mettman Ridge

The study area was clear cut and replanted with Douglas fir around the year 1994 (Montgomery and Dietrich, 1994). It has been examined by Schmidt *et al*. (2001) and Roering *et al*. (2003) from the scarps of landslides triggered during large storms in February and November of 1996 in the Oregon Coast Range. Although the majority of colluvium depths in landslides-prone areas range from 0.5 to 1.5 m, median rooting depths appear to be constrained to the upper 0.5 m of regolith. Though root strength provided significant apparent cohesion to the soil, it could not be easily accounted. An alternative way often adopted was to use a friction angle of 45°, increasing the soil strength to 1.4 times that of the actual frictional strength (Montgomery and Dietrich 1994; Rosso *et al*., 2006).

4.2.2 Mesh structure

Based on the DEM with a resolution of 2 m (available from http://calm.geo.berkeley.edu/geomorph//, the DEM shows no depression in the terrain), an irregular triangulated network was constructed to form a 3D finite-element mesh. The dimensions of the finite-element mesh are 747 m in the north-south direction (y axis), 682 m in the west-east direction (x axis), and 1.0 m in the vertical direction (z axis). The horizontal nodal spacing of the mesh is 5.0 m and the vertical nodal spacing is 0.05 m. The total number of nodes and elements in the mesh is 284277 and 532020, respectively.

4.2.3 Boundary conditions

The storm events observed to cause shallow landslide in this catchment had annual or biennial 24-h rainfall intensities of 50 to 75 mm/d (Montgomery, 1991; Montgomery and Dietrich, 1994; Torres *et al*., 1998). The rainfall condition in the simulation was set to be 1 d with rainfall intensity 50 mm/d. An unsaturated hydraulic conductivity function was determined by the method of van Genuchten (1980) using the parameters of transformed model parameters of α=0.075 and N=1.89 based on Torres *et al.* (1998) in Oregon Coast Range.

Based on the study of soil property in the Oregon Coast Range, soil internal friction angle of 45° was selected in the simulation, without consideration of soil and root cohesion. When bedrock is serving as the failure plane, the friction angle between the soil and bedrock is usually taken as smaller than that of soil (e.g., 30°), based on the experiment of measuring friction angle between the soil and concrete flume bed (Iverson *et al*., 1997; Montgomery *et al*., 2009). Considering many narrow ridge tops and steep slopes in the catchment, if the friction angle between the soil and bedrock is taken as 30°, most regions of the catchment is unconditionally unstable. In the present study, bedrock serving as failure is not considered and the friction angle between the soil and bedrock is set to be the same as soil.

The side and basal boundary condition is impermeable. The rainfall conditions, soil properties and other variables required to drive the model are summarized in Table 1.

4.2.4 Simulation results

During one day's rainfall with intensity of 50 mm/d, no surface overland flow was simulated.

Distribution of the slide angle, which takes from the vertical depth with the lowest FS value, is shown in Fig. 9. There is little difference in slide angle calculated by the hydraulic gradient and surface slope after one day's rainfall. The figure shows that the observed landslides took place in the slope larger than 36°, but not all the slopes with large slide angle would cause landslide.

The FS distribution estimated after one day's rainfall is shown in Fig. 10. The observed shallow landslides match the predicted unstable region well for both FS simulated by method I and method II. The simulated unstable regions also match the simulated unstable regions by SHALSTAB (Dietrich and Montgomery, 1998). Some observed landslides are located in the predicted stable regions because the effect of the upper and lateral landsliding force on the lower slope stability is not considered. The predicted unstable area by method I is larger than that by method II, which is mainly because of the difference in slide angle in FS calculation. When it is raining, the soil water content is changing dynamically and the spatial/temporal distribution of soil water content plays an important role in landslide processes. However, only the presented model (method I) can represent this transient process by consideration of the predominantly horizontal due to the initial condition and then increases when the soil gets wet, leading to hydraulic-gradient parallel sliding plane. In the specific case, the hydraulic gradient for the lower soil is

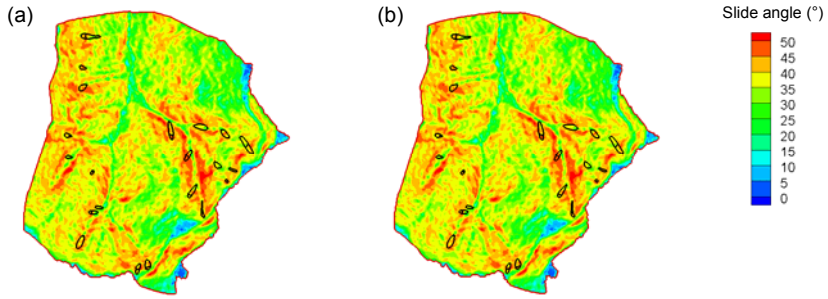

Fig. 9 Simulated slide angle after one day's rainfall with rainfall intensity of 50 mm/d by method I (a) and method II (b)
The black polygons are the observed landslides

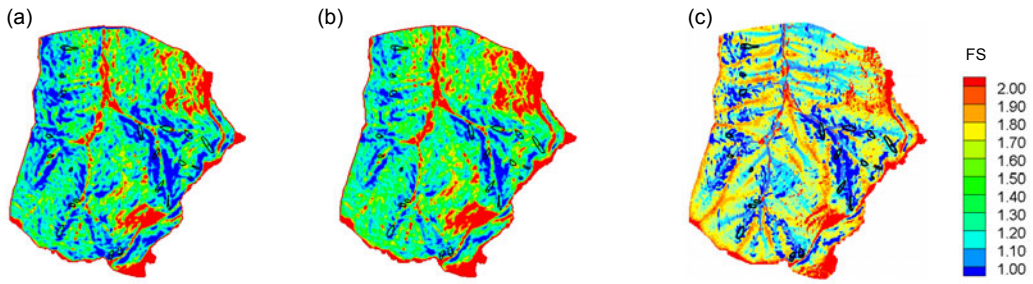

Fig. 10 Simulated FS after one day's rainfall with rainfall intensity of 50 mm/d by method I (a), method II (b) and SHALSTAB (c). The black polygons are the observed landslides

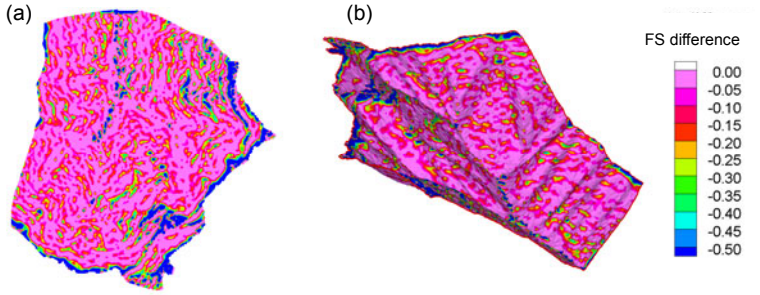

Fig. 11 Simulated FS difference after one day's rainfall with rainfall intensity of 50 mm/d
(a) Flat view; (b) 3D view

higher sliding angle which means lower FS value. In method II, the slide angle does not change and the FS value is the same from the surface to the groundwater table (i.e., Eqs. (16) and (17)) even though the soil is getting wet. The difference of FS simulated by method I and method II is shown in Fig. 11. Generally, FS simulated by method I is lower than that by method II, especially for the gentle region. This is important because the gentle slope still has the potential of landslide when the subsurface flow is strong. If using surface slope as the failure plane, this phenomenon may be neglected.

5 Discussion

Compared with other physically-based shallow landslide models, the present model uses a more rigorous physically-based hydrology model and a revised infinite slope stability model that can keep the original topography but provide reasonable landslide shape. The physically-based model has different simplifications in describing flow processes. Compared with the famous physically-based hydrology model SHE, which uses 2D overland flow, 1D channel flow, 3D saturated flow and 1D unsaturated flow, the hydrology model InHM in the present approach uses 2D overland flow, 2D channel flow, 3D saturated flow and unsaturated flow. In this sense, the present approach is more precise than the shallow landslide model based on the SHE family of models (Burton and Bathurst, 1998) as it can give better temporospatial distribution of water content, especially for high resolution DEM. Though these applications have shown some success in catchment scale modelling of shallow landslide triggered by rainfall, they have raised certain modelling difficulties, especially in representing the uncertainties associated with parameter evolution (Guimaraes *et al*., 2003).

In the present study, the selected catchment and synthetic single slopes have/exhibit hydraulic isotropy and homogeneity. This assumption simplifies the simulation but also makes the simulation result very similar to other models. The distribution of predicted FS for the selected catchment matches well with the predicted stability by SHALSTAB, as well as the observed landslide occurrence. Note that the rainfall conditions and initial conditions that triggered the observed landslides are not precisely recorded, and to some extent, these conditions are different from the initial and boundary conditions used in the present study. Considering some other unknowable factors (e.g., highly fractured bedrock), there appear to be some areas that are predicted to be unstable yet were not observed to be unstable and there also appear to be areas that were observed to fail yet the model predicts is stable.

The primary assumption in this study is that the failure plane is parallel to the hydraulic gradient. Though there are no field observations available at present that could support this assumption, it is our opinion, which is supported by the results of this study, that this assumption is appropriate for evaluating the spatially/temporally distributed susceptibility of shallow landslide.

For simple slopes or terrain without depressions, the hydraulic gradient is parallel to the surface slope on the whole, and the reported model generates similar FS distributions as methods assuming a surface-parallel sliding plane. However, the present model is capable of dealing with complex topography and no pre-processing of depressions and flat areas is needed, by which the original hydrologic response is preserved. Impacts of rolling topography and depressions are significant especially when the subsurface soil is getting saturated. Even with pre-processing of complex topographic feature, taking the surface slope as slide angle generally underestimates the slope stability. For heterogeneous porous media with fractured rock and fault zones, preferential flow paths through soil and rock contribute to the style and timing of landslide (Hencher, 2010). When the preferential flow path is served as the failure plane, it may not be parallel to the surface slope but will automatically be represented by the hydraulic gradient.

Although the presented model is able to generate spatial and temporal distributions of landslide susceptibility reasonably well, it is far from perfect. For infinite slopes, the hydraulic gradient depends on the slope angle, the groundwater specific discharge, and the distribution and anisotropy of the hydraulic conductivity (Iverson, 1990). When the hydraulic gradient is forced to be nearly horizontal, the model predicts a high FS, illustrating that the slope is stable. This is counterintuitive for steep slope because the flow lines in such cases are directed out of the slope,

thus significantly reducing the effective stress. For this situation, the present approach is not suitable. Some steep hydraulic gradients could happen because of the shape of the impermeable bottom boundary, leading to larger slide angles and unstable prediction. Surface slope may be used to validate the susceptibility of slope failure if an unusual hydraulic gradient occurs (e.g., hydraulic gradient significantly varies from surface slope). More field data is needed to calibrate the failure plane under different rainfall and topography conditions.

6 Conclusions

An infinite slope stability numerical model driven by a comprehensive physically-based hydrologic-response model has been developed and presented. The model's capability to estimate landslide susceptibility is illustrated by its application to two simple slopes and a small catchment study site in Mettman Ridge, Oregon. The landslides predicted by using the hydraulic gradient as the slide angle matches the observed landslides reasonably well. The presented approach is capable of not only predicting shallow landslide in catchment scale, as well as providing valuable detailed information such as landslide depth, but also dealing with complex topographic features such as depressions and flat areas without pre-procession.

Although the presented model is able to generate spatial and temporal distribution of landslide susceptibility, further improvement is still needed. Due to the limitations of available data, the soil properties and rainfall conditions have been taken to be homogeneous, which may not conform to the conditions of the observed landslides. Further work should also include producing detailed observed information of failure plane and failure depth, which are needed to calibrate the presented model and the assumption of hydraulic-gradient parallel slide angle.

References

Bathurst, J.C., Moretti, G., El-Hames, A., Moaven-Hashemi, A., Burton, A., 2005. Scenario modelling of basin-scale, shallow landslide sediment yield, Valsassina, Italian Southern Alps. *Natural Hazards and Earth System Science*, **5**(2):189-202. [doi:10.5194/nhess-5-189-2005]

Baum, R.L., Savage, W.Z., Godt, J.W., 2002. TRIGRS—A FORTRAN Program for Transient Rainfall Infiltration and Grid-Based Regional Slope-Stability Analysis. Open-File Report 02-424, US Department of the Interior and US Geological Survey.

Beville, S.H., Mirus, B.B., Ebel, B.A., Mader, G.G., Loague, K., 2010. Using simulated hydrologic response to revisit the 1973 Lerida Court landslide. *Environmental Earth Science*, **61**(6):1249-1257. [doi:10.1007/s12665-010-0448-z]

Bovolo, C.I., Bathurst, J.C., 2011. Modelling catchment-scale shallow landslide occurrence and sediment yield as a function of rainfall return period. *Hydrological Processes*, **21**(6):579-596. [doi:10.1002/hyp.8158]

Burroughs, E.R.Jr., Hammond, C.J., Booth, G.D., 1985. Relative Stability Estimation for Potential Debris Avalanche Sites Using Field Data. Proceedings of the International Symposium on Erosion, Debris Flow and Disaster Prevention, Erosion Control Society, Tokyo.

Burton, A., Bathurst, J.C., 1998. Physically based modelling of shallow landslide sediment yield at a catchment scale. *Environmental Geology*, **35**(2-3):89-99. [doi:10.1007/s002540050296]

Chang, C.L., 2007. Influence of moving rainstorms on watershed responses. *Environmental Engineering Science*, **24**(10):1353-1360. [doi:10.1089/ees.2006.0220]

Chen, C.Y., Chen, T.C., Yu, F.C., Lin, S.C., 2005. Analysis of time-varying rainfall infiltration induced landslide. *Environmental Geology*, **48**(4-5):466-479. [doi:10.1007/s00254-005-1289-z]

Claessens, L., Heuvelink, G.B.M., Schoorl, J.M., Veldkamp, A., 2005. DEM resolution effects on shallow landslide hazard and soil redistribution modelling. *Earth Surface Processes and Landforms*, **30**(4):461-477. [doi:10.1002/esp.1155]

Dietrich, W.E., Montgomery, D.R., 1998. SHALSTAB: A Digital Terrain Model for Mapping Shallow Landslide Potential. National Council of the Paper Industry for Air and Stream Improvement (NCASI), Technical Report.

Dietrich, W.E., de Asua, R.R., Coyle, J., Orr, B., Trso, M., 1998. A Validation Study of the Shallow Slope Stability Model, SHALSTAB, in Forested Lands of Northern California. Prepared for Louisiana-Pacific Corporation by Department of Geology and Geophysics, University of California, Berkeley and Stillwater Ecosystem, Watershed & Riverine Sciences, Berkeley, California.

Ebel, B.A., Loague, K., 2008. Rapid simulated hydrologic response within the variably saturated near surface. *Hydrological Processes*, **22**(3):464-471. [doi:10.1002/hyp.6926]

Ebel, B.A., Loague, K., Montgomery, D.R., Dietrich, W.E., 2008. Physics-based continuous simulation of long-term near-surface hydrologic response for the Coos Bay experimental catchment. *Water Resource Research*, **44**(7):W07417. [doi:10.1029/2007WR006442]

Ebel, B.A., Mirus, B.B., Heppner, C.S., VanderKwaak, J.E., Loague, K., 2009. First-order exchange coefficient coupling for simulating surface water-groundwater

interactions: Parameter sensitivity and consistency with a physics-based approach. *Hydrological Processes*, **23**(13):1949-1959. [doi:10.1002/hyp.7279]

Ebel, B.A., Loague, K., Borja, R.I., 2010. The impacts of hysteresis on variably-saturated hydrologic response and slope failure. *Environmental Earth Sciences*, **61**(6): 1215-1225. [doi:10.1007/s12665-009-0445-2]

Fernandes, N.F., Guimarães, R.F., Gomes, R.A.T., Vieira, B.C., Montgomery, D.R., Greenberg, H., 2004. Topographic controls of landslides in Rio de Janeiro: field evidence and modeling. *CATENA*, **55**(2):163-181. [doi:10.1016/S0341-8162(03)00115-2]

Guimaraes, R.F., Montgomery, D.R., Greenberg, H.M., Fernandes, N.F., Trancoso Gomes, R.A., de Carvalho, O.A., 2003. Parameterization of soil properties for a model of topographic controls on shallow landsliding: application to Rio de Janeiro. *Engineering Geology*, **69**(1-2):99-108. [doi:10.1016/s0013-7952(02)00263-6]

Hencher, S.R., 2010. Preferential flow paths through soil and rock and their association with landslides. *Hydrological Processes*, **24**(12):1610-1630. [doi:10.1002/hyp.7721]

Heppner, C.S., Loague, K., 2008. A dam problem: Simulated upstream impacts for a Searsville-like watershed. *Ecohydrology*, **1**(4):408-424. [doi:10.1002/eco.34]

Iverson, R.M., 1990. Groundwater flow fields in infinite slopes. *Geotechnique*, **40**(1):139-143. [doi:10.1680/geot.1990.40.1.139]

Iverson, R.M., 2000. landslide triggering by rain infiltration. *Water Resource Research*, **36**(7):1897-1910. [doi:10.1029/2000WR900090]

Iverson, R.M., Reid, M.E., LaHusen, R.G., 1997. Debris-flow mobilization from landslides. *Annual Review of Earth and Planetary Sciences*, **25**(1):85-138. [doi:10.1146/annurev.earth.25.1.85]

Kawagoe, S., Kazama, S., Sarukkalige, P.R., 2010. Probabilistic modelling of rainfall induced landslide hazard assessment. *Hydrology and Earth System Sciences Discussions*, **7**(1):725-766. [doi:10.5194/hessd-7-725-2010]

Lee, L.M., Gofar, N., Rahardjo, H., 2009. A simple model for preliminary evaluation of rainfall-induced slope instability. *Engineering Geology*, **108**(3-4):272-285. [doi:10.1016/j.enggeo.2009.06.011]

Loague, K., VanderKwaak, J.E., 2002. Simulating hydrological response for the R-5 catchment: comparison of two models and the impact of the roads. *Hydrological Processes*, **16**(5):1015-1032. [doi: 10.1002/hyp.316]

Loague, K., Heppner, C.S., Abrams, R.H., Carr, A.E., VanderKwaak, J.E., Ebel, B.A., 2004. Further testing of the Integrated Hydrology Model (InHM): event-based simulations for a small rangeland catchment located near Chickasha, Oklahoma. *Hydrological Processes*, **19**(7): 1373-1398. [doi:10.1002/hyp.5566]

Milledge, D.G., Griffiths, D.V., Lane, S.N., Warburton, J., 2012. Limits on the validity of infinite length assumptions for modelling shallow landslides. *Earth Surface Processes, and Landforms*, **37**(11):1158-1166. [doi:10.1002/esp.3235]

Minder, J.R., Roe, G.H., Montgomery, D.R., 2009. Spatial patterns of rainfall and shallow landslide susceptibility. *Water Resource Research*, **45**(4):W04419. [doi:10.1029/2008WR007027]

Mirus, B.B., Loague, K., VanderKwaak, J.E., Kampf, S.K., Burges, S.J., 2009. A hypothetical reality of Tarrawarra-like hydrologic response. *Hydrological Processes*, **23**(7): 1093-1103. [doi:10.1002/hyp.7241]

Montgomery, D.R., 1991. Channel Initiation and Landscape Evolution. PhD Thesis, University of California, Berkeley.

Montgomery, D.R., Dietrich, W.E., 1994. A physically based model for the topographic control on shallow landsliding. *Water Resource Research*, **30**(4):1153-1171. [doi:10.1029/93WR02979]

Montgomery, D.R., Schmidt, K.M., Greenberg, H.M., Dietrich, W.E., 2000. Forest clearing and regional landsliding. *Geology*, **28**(4):311-314. [doi:10.1130/0091-7613(2000)28<311:FCARL>2.0.CO;2]

Montgomery, D.R., Schmidt, K.M., Dietrich, W.E., MckKean, J., 2009. Instrumental record of debris flow initiation during natural rainfall: Implications for modeling slope. *Journal of Geophysical Research*, **114**(f1):F01031. [doi:10.1029/2008JF001078]

Ran, Q., 2006. Regional Scale Landscape Evolution: Physics-Based Simulation of Hydrologically-Driven Surface Erosion. PhD Thesis, Stanford University, USA.

Ran, Q., Heppner, C.S., VanderKwaak, J.E., Loague, K., 2007. Further testing of the integrated hydrology model (InHM): multiple-species sediment transport. *Hydrological Processes*, **21**(11):1522-1531. [doi:10.1002/hyp.6642]

Ran, Q., Loague, K., VanderKwaak, J.E., 2012. Hydrologic-response-driven sediment transport at a regional scale, process-based simulation. *Hydrological Processes*, **26**(2):159-167. [doi:10.1002/hyp.8122]

Renwick, W., 1982. Landslide morphology and processes on Santa Cruz Island, California. *Geografiska Annaler. Series A, Physical Geography*, **64**(3/4):149-159.

Roering, J.R., Schmidt, K.M., Stock, J.D., Dietrich, W.E., Montgomery, D.R., 2003. Shallow landsliding, root reinforcement, and the spatial distribution of trees in the Oregon Coast Range. *Canadian Geotechnical Journal*, **40**(2):237-253. [doi:10.1139/T02-113]

Rosso, R., Rulli, M.C., Vannucchi, G., 2006. A physically based model for the hydrologic control on shallow landsliding. *Water Resource Research*, **42**(6):W06410. [doi:10.1029/2005WR004369]

Schmidt, K.M., Roering, J.R., Stock, J.D., Dietrich, W.E., Montgomery, D.R., Schaub, T., 2001. The variability of root cohesion as an influence on shallow landslide susceptibility in the Oregon Coast Range. *Canadian Geotechnical Journal*, **38**(5):995-1024. [doi:10.1139/cgj-38-5-995]

Schroeder, W.L., Alto, J.V., 1983. Soil properties for slope stability analysis; Oregon and Washington Coastal Mountains. *Forest Science*, **29**(4):823-833.

Torres, R., Dietrich, W.E., Montgomery, D.R., Anderson, S.P., Loague, K., 1998. Unsaturated zone processes and the hydrologic response of a steep, unchanneled catchment. *Water Resources Research*, **34**(8):1865-1879. [doi:10.1029/98wr01140]

Tsai, T.L., Yang, J.C., 2006. Modeling of rainfall-triggered shallow landslide. *Environmental Geology*, **50**(4):525-534. [doi:10.1007/s00254-006-0229-x]

Tsai, T.L., Chen, H.E., Yang, J.C., 2008. Numerical modeling of rainstorm-induced shallow landslides in saturated and unsaturated soils. *Environmental Geology*, **55**(6):1269-1277. [doi:10.1007/s00254-007-1075-1].

VanderKwaak, J.E., 1999. Numerical Simulation of Flow and Chemical Transport in Integrated Surface-Subsurface Hydrologic Systems. PhD Thesis, University of Waterloo.

VanderKwaak, J.E., Loague, K., 2001. Hydrologic-response simulations for the R-5 catchment with a comprehensive physics-based model. *Water Resources Research*, **37**(4):999-1013. [doi:10.1029/2000WR900272]

van Genuchten, M.T., 1980. A closed-form equation for predicting the hydraulic conductivity of unsaturated soils. *Soil Science Society of America Journal*, **44**(5):892-898. [doi:10.2136/sssaj1980.03615995004400050002x]

Yee, C., Harr, R., 1977. Influence of soil aggregation on slope stability in the Oregon Coast Ranges. *Environmental Geology*, **1**(6):367-377. [doi:10.1007/BF02380505]